International Journal of Heat and Fluid Flow 31 (2010) 179–190

Contents lists available at ScienceDirect

International Journal of Heat and Fluid Flow

journal homepage: www.elsevier.com/locate/ijhff

# Investigation of turbulent mixed convection of air flow in vertical tubes using a zonal turbulence model

Mehdi Shahraeeni *, Mehrdad Raisee

*School of Mechanical Engineering, College of Engineering, University of Tehran, Tehran, Iran*

ARTICLE INFO

*Article history:*
Received 15 August 2008
Received in revised form 5 December 2009
Accepted 8 December 2009
Available online 13 January 2010

*Keywords:*
Mixed convection
Upward and downward flow
Turbulence
Zonal $k$–$\varepsilon$ model

ABSTRACT

Fluid flow and heat transfer in a vertical tube under constant heat flux have been studied and the effect of buoyancy force on the heat transfer coefficient is investigated. The finite volume method is used to study turbulent flow in both upward and downward directions. For the turbulence modeling, a zonal $k$–$\varepsilon$ model is employed and the numerical results are compared with available experimental data. The results of the simulation show that for the downward flow, heat transfer is enhanced and for strong buoyancy force, flow reversal is observed. In contrast, for the heated upward flow, heat transfer can be either impaired or enhanced by the buoyancy force depending on its strength. Partial laminarization is caused by the buoyancy in the case of modest buoyancy force. For the condition of stronger buoyancy force, a sudden decrease in the fully-developed Nusselt number is evident in the experimental data and well predicted by the numerical solution. In general, the quantitative agreement between the numerical results and the experimental data is satisfactory.



## 1. Introduction

Extensive practical applications of mixed convection including the cooling of nuclear reactors and electronic components, internal cooling system of turbine blades and compact heat exchangers caused a huge attention to be directed on the subject. Although the geometry involved in most applications are relatively simple, predicting heat transfer phenomena of such flows is very complex. The complexities are associated with the behavior of fluid flow in the near-wall region. In the case of laminar mixed convection, the near-wall velocity is increased in buoyancy-aided flows and decreased in buoyancy-opposed flows. Thus, heat transfer is enhanced and impaired respectively. In contrast for turbulent flow, the interaction between the velocity field and the rate of turbulence production in the near-wall region determines the impairment or enhancement of the rate of heat transfer. While the buoyancy force reduces advection for downward flow, the higher level of turbulence production in the near-wall region always improves the wall heat transfer. In the buoyancy-aided case, advection in the near-wall region is increased. However, the turbulence production is reduced due to the decreased level of shear stress in the same region. The net result is impairment of the wall heat transfer. A complete condition of laminarization is achieved when the shear stress in the near-wall region falls as a result of increased buoyancy force. Therefore, any further increase of buoyancy force raises the rate of turbulence production and results in heat transfer enhancement.

Several studies have been conducted on the implementation of various turbulence closures to take into account mixed convection phenomena. A comprehensive review of these models up to the ninetieth is presented by Jackson et al. (1989). Tanaka et al. (1987) examined turbulent mixed convection flow in tubes using Reichardt's (1961) eddy diffusivity model with modifications. The wall temperature distributions obtained for a vertical heated tube were in contradiction with the experimental results concluding that simple turbulence models are not reliable to model mixed convection. Cotton (1987) used the low-Reynolds-number $k$–$\varepsilon$ turbulence model of Launder and Sharma (1974) for buoyancy-aided mixed convection in the vertical tubes. The model was applied for simulating an earlier experiment on buoyancy-aided mixed convection (Cotton and Jackson (1990)). The simulations were generally found to be in acceptable agreement with the experimental data of Carr et al. (1973) and Steiner (1971). Later, a comparative study of the performance of a number of turbulence models was carried out by Mikielewicz (1994). The study considered the comparison of the efficiency of turbulence models in predicting heat transfer with experimental data. It was found that the Launder and Sharma (1974) and the Chien (1982) low-Re models generally perform better than the rest. Cotton and Kirwin (1995) reported a variant of the Launder and Sharma (1974) low-Reynolds-number $k$–$\varepsilon$ turbulence model. They developed a model on the basis of an empirical optimization procedure. The results of the model were generally in better agreement with the DNS data for forced

* Corresponding author. Tel.: +1 250 575 8360; fax: +1 250 807 9850.
*E-mail address:* mehdi128@interchange.ubc.ca (M. Shahraeeni).

0142-727X/$ - see front matter © 2009 Elsevier Inc. All rights reserved.
doi:10.1016/j.ijheatfluidflow.2009.12.004

**Nomenclature**

| | |
|---|---|
| $b$ | constant in the Sutherland correlation |
| Bo | buoyancy parameter, $Gr/(Re^{3.425}Pr^{0.8})$ |
| $D$ | tube diameter |
| Gr | Grashof number, $\beta g D^4 q''_w/\kappa\nu^2$ |
| $k$ | turbulent kinetic energy |
| Nu | Nusselt number, $q''_w D/\kappa(T_w - T_b)$ |
| $Nu_f$ | Nusselt number for forced convection |
| $P_k$ | turbulence energy production |
| Pr | Prandtl number, $\mu c_p/\kappa$ |
| $q''_w$ | convective heat flux from the wall |
| $r$ | radial coordinate |
| $r_c$ | radius of curvature |
| Re | Reynolds number, $U_b D/\nu$ |
| $S$ | constant in the Sutherland correlation |
| $S^\Psi$ | general source term |
| $T$ | temperature |
| $-\rho\overline{u_i u_j}$ | Reynolds stress tensor components |
| $\rho C_p \overline{u_i t}$ | turbulent heat flux |
| $U_j$ | mean velocity component |
| $y$ | radial distance from the wall |
| $y^*$ | non-dimensional distance from the wall based on $k$, $yk^{1/2}/\nu$ |
| $y^+$ | non-dimensional distance from the wall, $y(\lvert\tau_w\rvert/\rho)^{1/2}/\nu$ |
| $z$ | axial distance from the beginning of the heating zone |

*Subscripts*

| | |
|---|---|
| b | bulk fluid |
| $f$ | forced convection |
| I | the closest node to the wall |
| in | inlet of the tube |
| w | wall |

*Greek symbols*

| | |
|---|---|
| $\beta$ | coefficient of thermal expansion |
| $\Gamma^\Psi$ | coefficient of effective diffusion |
| $\varepsilon$ | dissipation rate of $k$ |
| $\kappa$ | thermal conductivity |
| $\nu$ | kinematic viscosity |
| $\nu_t$ | turbulent kinematic viscosity |
| $\sigma_T$, $\sigma_k$, $\sigma_\varepsilon$ | turbulent Prandtl number for temperature, $k$ and $\varepsilon$ |
| $\Psi$ | general dependent variable |

convection. However, in some cases under study, the performance of the original model of Launder and Sharma (1974) was reported to be better than the modified model. Behzadmehr et al. (2003) conducted a study of mixed convection of air flow in a vertical tube. The study was limited to upward direction for two Reynolds numbers of Re = 1000 and 1500 over a range of Grashof numbers. The Launder and Sharma low-Re $k$–$\varepsilon$ model was implemented and for each Reynolds number, they found two critical Grashof numbers corresponding to laminar-turbulent transition. More recently, Kenjeres et al. (2005) proposed a quasi-linear model for turbulent heat flux. They considered a buoyancy-extended stress–strain model coupled with five equations ($k$—$\varepsilon$—$\bar{v}^2$—$f$—$\bar{\theta}^2$) and applied it to a wide range of natural and mixed convection flows. The results were in fairly good agreement with experimental data.

Direct numerical simulation (DNS) has also been used to study mixed convection in the vertical channels. One of the earliest studies was conducted by Kasagi and Nishimura (1997). They primarily fixed the Reynolds number (based on the channel half-width and the friction velocity) at 150, while the Grashof number varies from 0 to $1.6 \times 10^6$. They found that the opposing and aiding buoyancy forces affect the turbulent statistics and the quasi-coherent structures in much the same way as the wall injection/suction and the Lorenz force. As a result the near-wall force balance is modified causing heat transfer enhancement or impairment. You et al. (2003) studied turbulent mixed convection in a heated vertical tube using DNS. The fluid properties were assumed to be uniform and Boussinesq's approximation was used. They confirmed the validity of the log laws of the mean velocity and the temperature profiles for downward heated flow. The same research group in Bae et al. (2005) conducted a DNS study of mixed convection heat transfer of carbon dioxide at supercritical pressure. They reported deformation of the mean velocity profile into an M-shaped one for upward flow, and the variation of velocity fluctuation both in sign and magnitude causing impairment of heat transfer. Recently, Kim et al. (2008) presented an assessment of the performance of a variety of turbulence models in simulating buoyancy-aided turbulent mixed convection in vertical tubes. They compared the prediction of RANS-based models with available DNS results. They showed that indirect influence of the buoyancy force on the turbulence in a heated vertical tube is the dominant mechanism which causes laminarization and deterioration of heat transfer.

In the present study, the zonal modeling approach is employed to investigate the influence of the buoyancy force on the fluid flow and heat transfer. The zonal $k$–$\varepsilon$ model is applied for both aiding and opposing turbulent flows inside a vertical tube with constant heat flux. This modeling approach allows the resolution of the mean motion across the sub-layer region without the need for very fine grid resolutions associated with low-Reynolds-number models, in which the dissipation rate equation is integrated up to the wall (Raisee, 1999). Therefore, the model is computationally more economical. Moreover, the use of the zonal $k$–$\varepsilon$ model for the prediction of mixed convection in vertical tubes has not been previously investigated.

## 2. Flow geometry

In order to validate the numerical results presented in this paper, the experimental results of Li and Jackson (1999) are employed. Fig. 1a shows the general arrangement of the test configuration for the upward flow with an unheated development section. A blower delivers laboratory air through a flexible duct to the entry box with a honeycomb arrangement inside to straighten the flow. A long unheated development section makes the flow to be fully-developed at the inlet of the heated section. After passing the heated section, air is finally exhausted through a flow metering nozzle. Full details of the experiment and its setup can be found in Li and Jackson (1999). The schematic of 2D axi-symmetric flow geometry considered for analysis of upward and downward flows is shown in Fig. 1b. The only difference between the two flows is the sign of the gravitational force which is in the same direction of the main flow for downward case, while it opposes the main flow for upward case.

In order to investigate the effect of the buoyancy force on the rate of heat transfer, three different cases are presented and discussed. As shown in Table 1, each test case is associated with a certain value of Bo parameter, which combines Grashof number, Reynolds number and Prandtl number in the form of $Gr/(Re^{3.425}Pr^{0.8})$ to characterize the strength of buoyancy influence

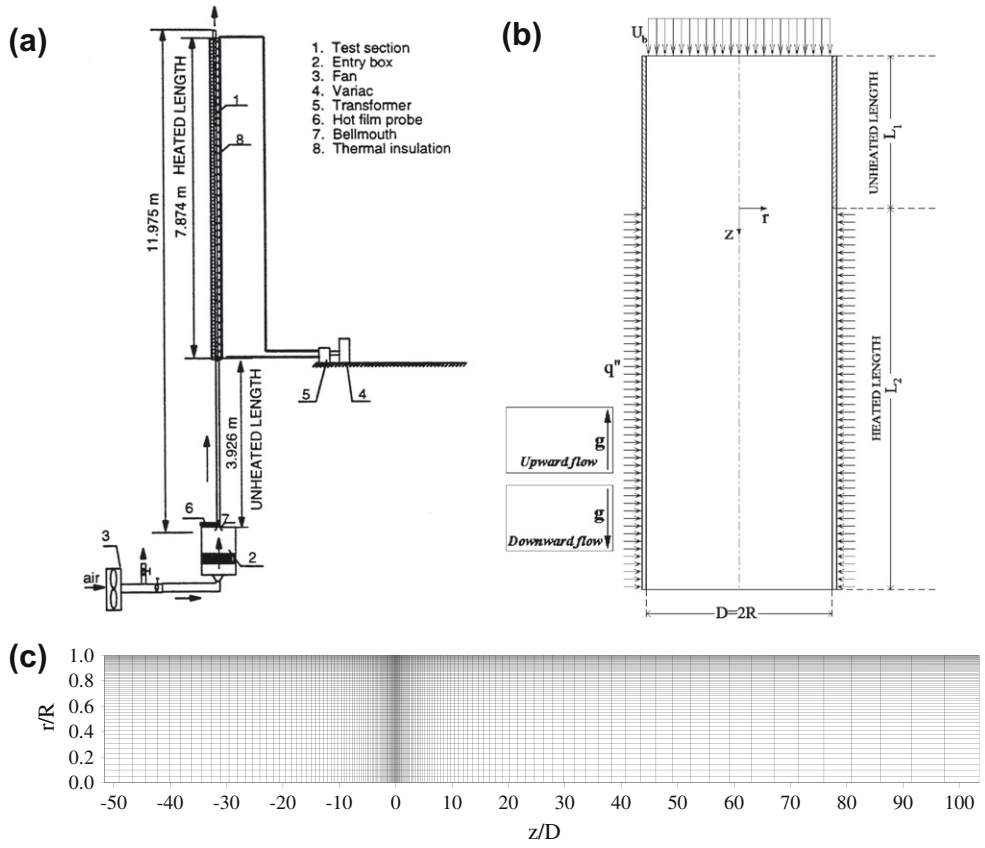


**Fig. 1.** (a) General arrangement of Li and Jackson (1999) experiment, (b) geometry model and (c) computational mesh with 150 × 60 nodes.

**Table 1**
Details of cases examined.

| Case | Re | Gr | Bo | Status |
|---|---|---|---|---|
| (a) | 38075 | $2.97 \times 10^8$ | 0.0064 | Negligible buoyancy force |
| | 24591 | $2.423 \times 10^8$ | 0.0233 | |
| (b) | 7220 | $1.145 \times 10^8$ | 0.7317 | Small buoyancy force |
| (c) | 2133 | $8.247 \times 10^7$ | 34.3111 | Strong buoyancy force |

(Li and Jackson, 1999). For the first test cases, where Bo = 0.0064 and 0.0233, the effect of buoyancy force is negligible compared to the viscous and inertia forces. For the second case (Bo = 0.7317), the buoyancy force is neither negligible nor dominant and for the last test case with Bo = 34.3111, the buoyancy force dominates the flow in the near-wall region which significantly affects the rate of heat transfer.

## 3. Governing equations

### 3.1. Mean flow and energy equations

For stationary turbulent flow, the time-averaged governing equations of mass, momentum and energy are written as:

$$\frac{\partial U_j}{\partial x_j} = 0 \tag{1}$$

$$\frac{\partial}{\partial x_j}(U_i U_j) = -\frac{1}{\rho}\frac{\partial P}{\partial x_i} + \frac{\partial}{\partial x_j}\left(\nu \frac{\partial U_i}{\partial x_j} - \overline{u_i u_j}\right) + f_i \tag{2}$$

$$\frac{\partial (U_j T)}{\partial x_j} = \frac{\partial}{\partial x_j}\left(\frac{\nu}{\mathrm{Pr}}\frac{\partial T}{\partial x_j} - \overline{u_j t}\right) \tag{3}$$

where $\rho$, $\nu$ and Pr are the density, kinematic viscosity and Prandtl number respectively, and $f_i$ represents the body force.

For the flows considered in this study, the Mach number is sufficiently low, and thus the flows are assumed to be incompressible. However, the variation of air viscosity with local temperature is taken into account using the Sutherland (1893) correlation:

$$\mu = \frac{b T^{\frac{3}{2}}}{S + T} \tag{4}$$

in which $b = 1.458 \times 10^{-6}$ kg/(m s K$^{1/2}$) and $S = 110.4$ K are constants for air.

### 3.2. Turbulence modeling

In this study, a zonal low-Re $k$–$\varepsilon$ model is implemented for investigation of mixed convection in vertical tubes. The model was successfully employed for rotating cavities by Iacovides and Theofanopoulos (1991) and also Iacovides and Chew (1993). However, this turbulence modeling approach has not been used for mixed convection problems.

In the zonal $k$–$\varepsilon$ model, the computational domain is divided into two parts: the fully-turbulent region and the low-Re near-wall region. In the fully-turbulent region, the standard high-Re version of $k$–$\varepsilon$ model is used, while in the near-wall region a low-Re version of one-equation model is employed. This approach allows the resolution of mean flow across the viscous sub-layer without the need to use a very fine near-wall grid (Raisee, 1999). The Reynolds stresses $-\rho\overline{u_i u_j}$ and the turbulent heat fluxes $\rho C_P \overline{u_i t}$ are obtained via the well-known eddy-viscosity and gradient-diffusion hypotheses:

**Table 2**
Constants in the standard high-Re model.

| $C\mu$ | $C_{\varepsilon 1}$ | $C_{\varepsilon 2}$ | $\sigma_k$ | $\sigma_\varepsilon$ | $\sigma_T$ |
|---|---|---|---|---|---|
| 0.09 | 1.44 | 1.92 | 1.0 | 1.3 | 0.9 |

$$\overline{u_i u_j} = -\nu_t\left(\frac{\partial U_i}{\partial x_j}+\frac{\partial U_j}{\partial x_i}\right)+2/3\delta_{ij}k \tag{5}$$

$$\overline{u_i t} = -\frac{\nu_t}{\sigma_T}\frac{\partial T}{\partial x_i} \tag{6}$$

The gradient-diffusion hypothesis implies that the heat flux ($\overline{u_i t}$) is aligned with the mean temperature gradient vector ($\partial T/\partial x_i$). Constant $\sigma_T$ is turbulent Prandtl number given in Table 2.

In the fully-turbulent region, the turbulent viscosity ($\nu_t$) that appears in Eqs. (5) and (6) is obtained from the turbulent kinetic energy, $k$, and its dissipation rate, $\varepsilon$:

$$\nu_t = c_\mu\frac{k^2}{\varepsilon} \tag{7}$$

In order to evaluate the distribution of $k$ and $\varepsilon$, two additional transport equations have to be solved:

$$\frac{\partial}{\partial x_j}(U_j k) = \frac{\partial}{\partial x_j}\left[\left(\nu+\frac{\nu_t}{\sigma_k}\right)\frac{\partial k}{\partial x_j}\right]+P_k-\varepsilon \tag{8}$$

$$\frac{\partial}{\partial x_j}(U_j \varepsilon) = \frac{\partial}{\partial x_j}\left[\left(\nu+\frac{\nu_t}{\sigma_\varepsilon}\right)\frac{\partial \varepsilon}{\partial x_j}\right]+c_{\varepsilon 1}\frac{\varepsilon}{k}P_k-c_{\varepsilon 2}\frac{\varepsilon^2}{k} \tag{9}$$

where the production term is obtained via:

$$P_k = -\overline{u_i u_j}\frac{\partial U_i}{\partial x_j} \tag{10}$$

In the low-Re near-wall region, Eqs. (8) and (10) are still used to obtain the distribution of $k$, but the dissipation rate ($\varepsilon$) and the turbulent viscosity ($\nu_t$) are obtained from the algebraic expressions (11) and (12), proposed by Wolfshtein (1969), that rely on the prescribed length scales $\ell_\varepsilon$ and $\ell_\mu$:

$$\varepsilon = k^{3/2}/\ell_\varepsilon \tag{11}$$

$$\nu_t = c_\mu \ell_\mu \sqrt{k} \tag{12}$$

The length scales $\ell_\varepsilon$ and $\ell_\mu$ are obtained from the near-wall distance ($y^*$), according to:

$$\ell_\varepsilon = 2.55\ y[1-\exp(-0.236y^*)] \tag{13}$$

$$\ell_\mu = 2.55\ y[1-\exp(-0.016y^*)] \tag{14}$$

where $y^* \equiv yk^{1/2}/\nu$ is the dimensionless distance from the wall that is used to introduce the damping effect of the wall on turbulence.

## 4. Numerical method and boundary conditions

The tensorial form of the governing equations of the mean flow, temperature and turbulence is presented in the previous section. The general form of these equations in the polar-cylindrical coordination system for a dependent variable $\Psi$ is written as:

$$\left[\frac{\partial}{\partial z}(\rho r_c U\Psi)+\frac{\partial}{\partial r}(\rho r_c V\Psi)\right] = \left[\frac{\partial}{\partial z}\left(\Gamma^\Psi r_c\frac{\partial \Psi}{\partial z}\right)+\frac{\partial}{\partial r}\left(\Gamma^\Psi r_c\frac{\partial \Psi}{\partial r}\right)\right]+r_c S^\Psi \tag{15}$$

where $\Psi$ represents velocity components, temperature and turbulent quantities ($k$ and $\varepsilon$), $z$ and $r$ are the coordinates in the axial and radial directions respectively. $\Gamma^\Psi$ is the effective diffusion coefficient and $S^\Psi$ denotes the source term in each transport equation. For the momentum equation, $S^\Psi$ includes the pressure gradient as well as the buoyancy force. To take into account the effect of buoyancy, the pressure source term in the axial momentum equation is modified as follows:

$$S^P = -\frac{\partial P}{\partial z}-\rho g_e(\beta T - T_{\text{ref}}) \tag{16}$$

in which, $\partial P/\partial z$ is the pressure gradient and $\rho g_e\beta(T-T_{\text{ref}})$ is the force due to buoyancy. For the upward flow, where the buoyancy force is aiding the main flow, $g_e = -g$, while for the downward flow, $g_e = +g$.

Eq. (15) is discretized using finite-volume methodology on a semi-staggered grid system. The velocity components ($U$ and $V$) are located at the same nodal positions which are staggered relative to the pressure nodes. All of the turbulent quantities and scalars are stored at the pressure nodes. The hybrid differencing scheme is used for approximating the convective terms. The pressure field is linked to the velocity field using the well-known SIMPLE pressure correction algorithm. To avoid any instabilities associated with the pressure–velocity decoupling, the Rhie and Chow (1983) interpolating scheme is employed. Assuming a completely vertical flow, the symmetry boundary condition is used along the axis of the tube. The radial component of the velocity is set to zero on this boundary and the values of other variables are set equal to the values of adjacent nodes inside the domain. Since the turbulence model used in this study is a low-Reynolds-number model, it is not necessary to use a particular method such as wall-functions for the wall boundary. The velocity, the pressure correction term and the turbulent kinetic energy are equal to zero on the solid wall. The boundary condition for the energy equation on the wall is obtained using Fourier's law:

$$q''_{\text{w}} = -\kappa\frac{\partial T}{\partial r} \tag{17}$$

The temperature gradient is set to zero in the unheated section and is calculated using following equation in the heated region:

$$T_{\text{w}} = T_I+\frac{q''_{\text{w}}\text{Pr}\Delta r}{\mu c_p} \tag{18}$$

where $T_I$ is the temperature of the closest node to the wall and $\Delta r$ is the distance to the wall.

In order to be consistent with the experiment of Li and Jackson (1999), the velocity and temperature profile are assumed to be uniform at the tube entrance and fully-developed flow and thermal boundary conditions are assumed at the exit. As for the turbulent kinetic energy and its dissipation rate, the following boundary conditions are used at the inlet (Raisee et al., 2006):

$$k_{\text{in}} = (0.08U_{\text{in}})^2, \quad \varepsilon_{\text{in}} = k_{\text{in}}^{3/2}/\ell \tag{19}$$

where $U_{\text{in}}$ is the inlet velocity and $\ell = 0.1\ D$.

A non-uniform mesh with 150 axial nodes and 60 radial nodes is used (Fig. 1c). Close to the heating zone ($z/D = 0$) a finer mesh is used to capture high gradients. As flow develops and the thermal boundary layer grows in thickness, the necessity to capture high details of flow in the axial direction is decreased, and the mesh becomes coarser. For the radial direction, the nodes are clustered enough near the wall as the gradients are high. In order to capture the details of the flow in the viscous sub-layer, 20 grid nodes are considered near the solid wall. The value of turbulent Reynolds number ($y^*$) at the interface between the inner layer and the fully-turbulent region is approximately 100. The $y^+$ values for the nodes adjacent to the wall are lower than one, ensuring that the near-wall grids are positioned within the viscous sub-layer. In order to show that the results obtained using the $150\times 60$ mesh are grid-independent, numerical results for a coarser mesh

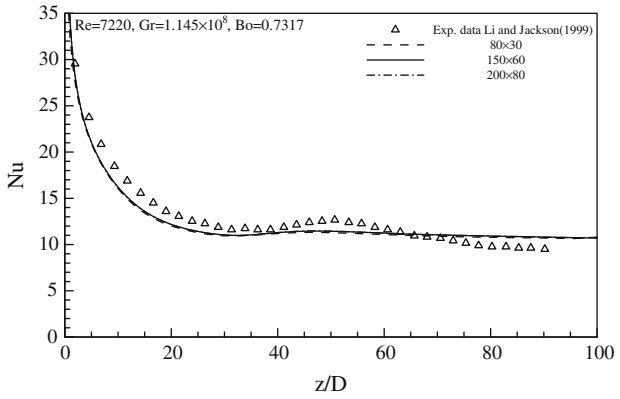


**Fig. 2.** Effect of different grids on distribution of local Nusslet number for upward flow.

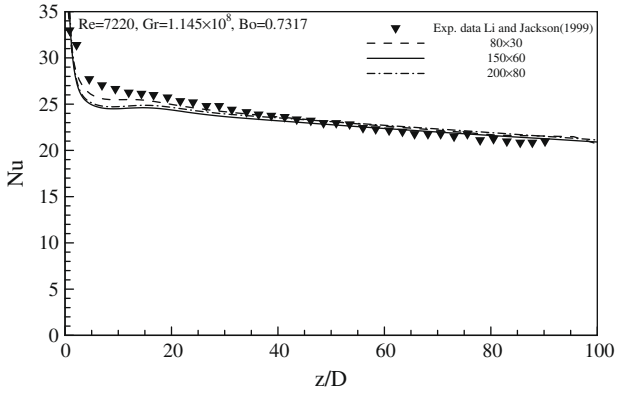


**Fig. 3.** Effect of different grids on distribution of local Nusslet number for downward flow.

($80 \times 30$) and a finer mesh ($200 \times 80$) are also obtained. The distribution of Nusselt number for buoyancy number (Bo) of 0.7317, are respectively shown in Figs. 2 and 3 for the upward and downward flows. For the upward flow, the results of three meshes are identical. For downward flow, differences are observed between the results obtained using the coarse mesh ($80 \times 30$) and those returned by the fine mesh ($150 \times 60$) in the developing region. Further grid refinement has no major effect on the prediction of the heat transfer rate.

## 5. Results and discussion

### 5.1. Case (a): negligible buoyancy force

To assess the validity of the in-house numerical code used in this study, the numerical results for upward flow at Re = 38075 and $Gr = 2.97 \times 10^8$ and downward flow at Re = 24591and $Gr = 2.423 \times 10^8$ are studied. The buoyancy parameters are 0.0064 and 0.0233 respectively, showing that the effects of buoyancy are negligible and heat transfer can be approximated by forced convection. The numerical results are compared with existing semi-empirical correlations for forced convection and the experimental results of Li and Jackson (1999). Petukhov et al. (1972) suggested the following correlations for the friction factor ($f$) and the Nusselt number (Nu) for fully-developed turbulent forced convection through the tubes:

$$f = \left[1.82 \ln\left(\frac{\mathrm{Re}}{8.0}\right)\right]^{-2} \tag{20}$$

$$\mathrm{Nu}_{p_{cp}} = \frac{\mathrm{Re} \cdot \mathrm{Pr}\left(\frac{f}{8}\right)}{1.07 + \frac{900}{\mathrm{Re}} - \frac{0.63}{(1+10\mathrm{Pr})} + 12.5\sqrt{\frac{f}{8}}\left(\mathrm{Pr}^{\frac{2}{3}} - 1\right)} \tag{21}$$

The correlation was subsequently modified by Petukhov et al. (1972) with the following coefficient considering the effect of entrance region:

$$C_{\mathrm{Therm}} = 1.0 + 0.48\left[1.0 + \frac{3600}{\mathrm{Re}\sqrt{z/D}}\right]\frac{\exp(-0.17z/D)}{(z/\mathrm{D})^{0.25}} \tag{22}$$

In Fig. 4, the computed Nusselt number for upward flow at Re = 38075 and $Gr = 2.97 \times 10^8$ is compared with the experimental results and the semi-empirical correlation for developing flows (Eqs. (20)–(22)). The Nu number distribution obtained using the zonal $k$–$\varepsilon$ model is in close agreement with experimental data and the correlation of forced convection. The same comparison is made for downward flow at Re = 24591 and $Gr = 2.423 \times 10^8$ in Fig. 5. Although some differences are observed between the experimental results and the numerical solution, the overall agreement is satisfactory. The results indicate that the assumption of forced convection at negligible values of buoyancy parameter is valid.

### 5.2. Case (b): small buoyancy force

For the Reynolds number of Re = 7220 and Grashof number of $Gr = 1.145 \times 10^8$, the buoyancy parameter is Bo = 0.7317. The buoyancy parameter, as discussed earlier, represents the effect of buoyancy force in the flow with respect to the other existing forces

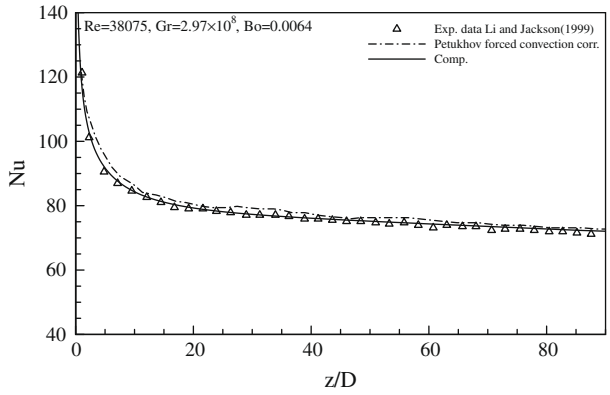


**Fig. 4.** Comparison of predicted Nusselt number from the current model with experimental data for upward flow.

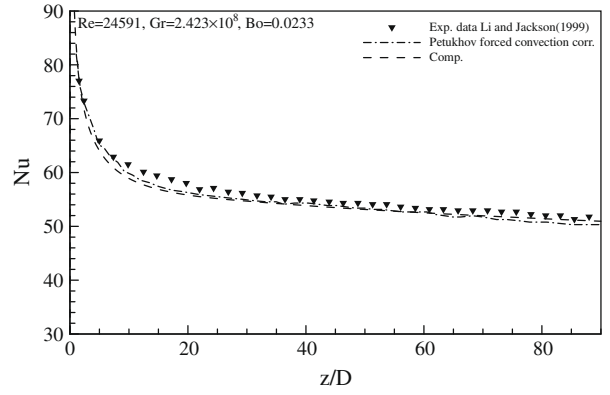


**Fig. 5.** Comparison of predicted Nusselt number from the current model with experimental data for downward flow.

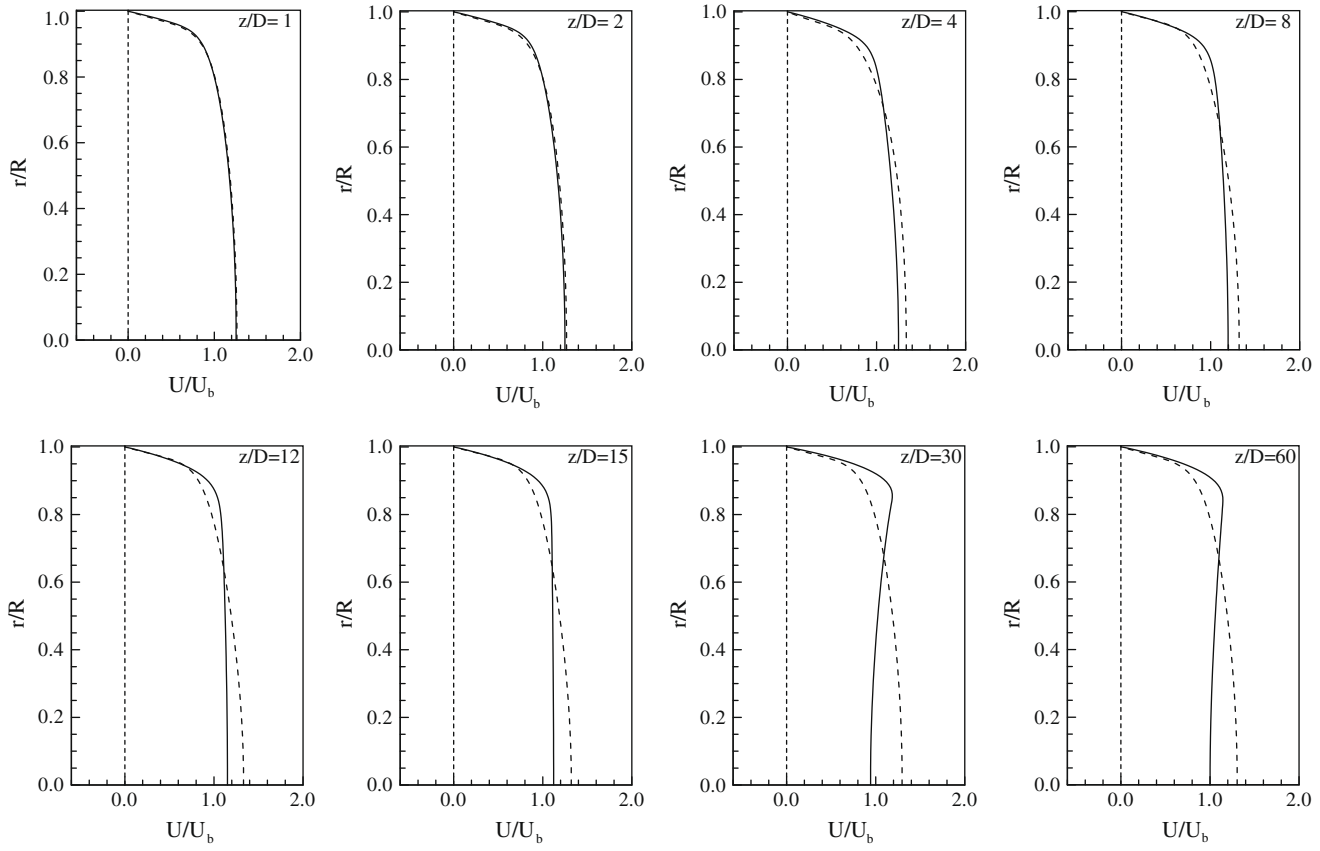


**Fig. 6.** Normalized velocity profiles for upward (solid line) and downward (dashed line) flows at different cross sections (Re = 7220, Gr = $1.145 \times 10^8$, Bo = 0.7317).

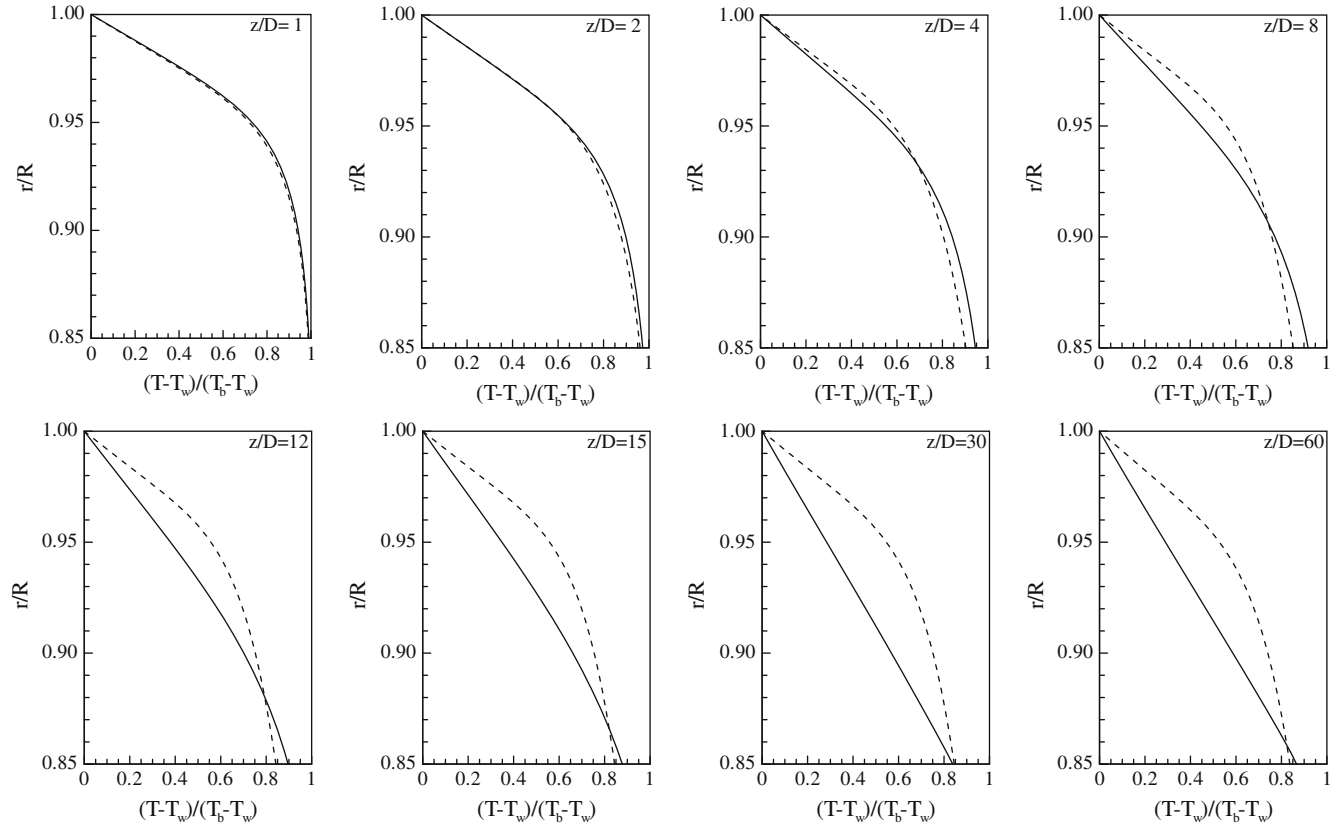


**Fig. 7.** Normalized temperature profiles for upward (solid line) and downward (dashed line) flows at different cross sections (Re = 7220, Gr = $1.145 \times 10^8$, Bo = 0.7317).

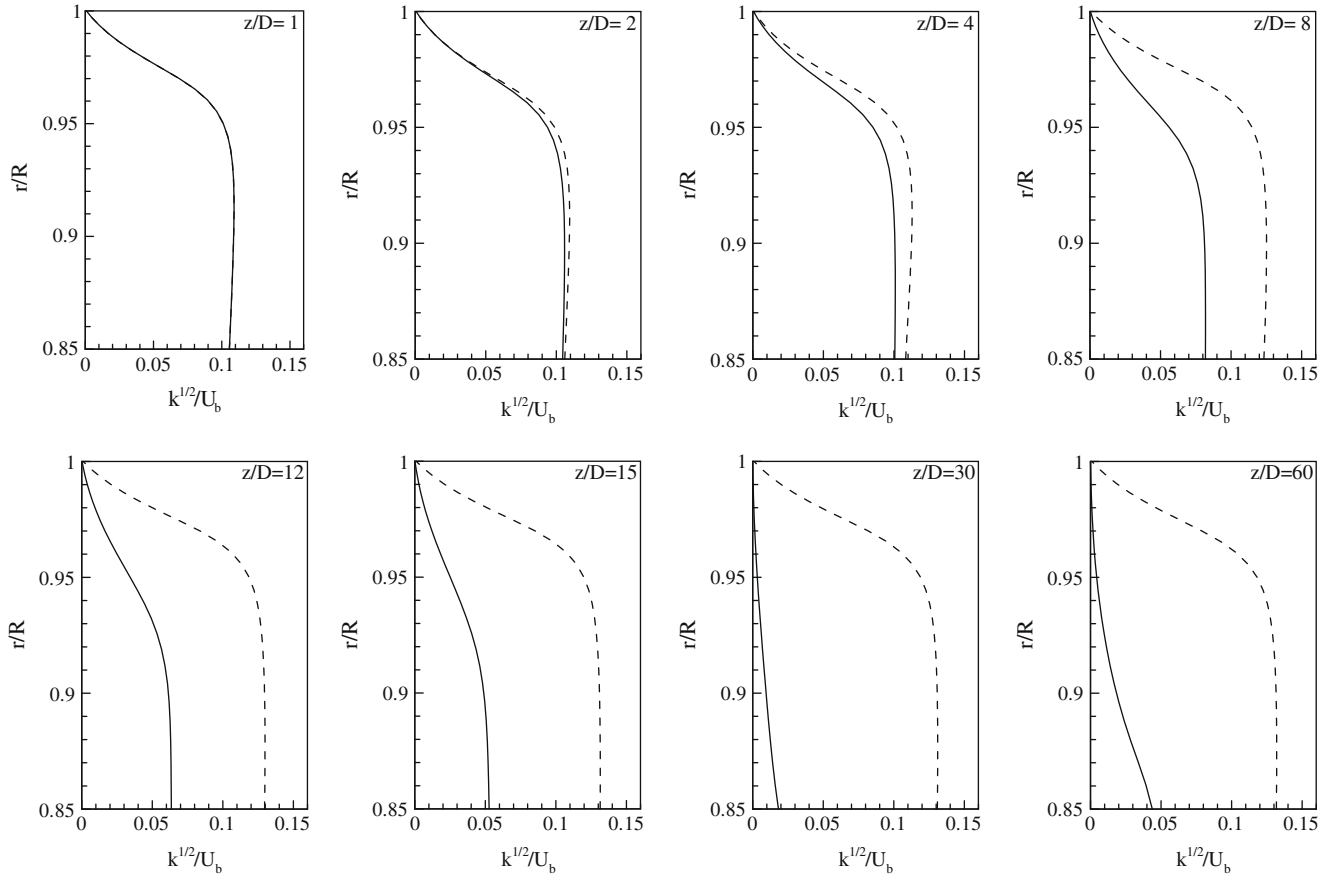


**Fig. 8.** Normalized turbulent kinetic energy profiles for upward (solid line) and downward (dashed line) flows at different cross sections (Re = 7220, Gr = $1.145 \times 10^8$, Bo = 0.7317).

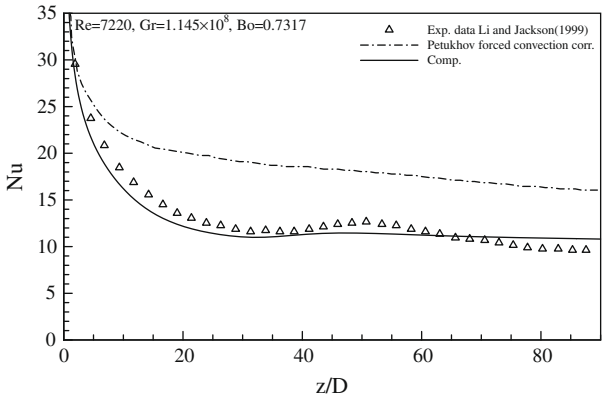


**Fig. 9.** Comparison of predicted Nusselt number from the current model with experimental data for upward flow.

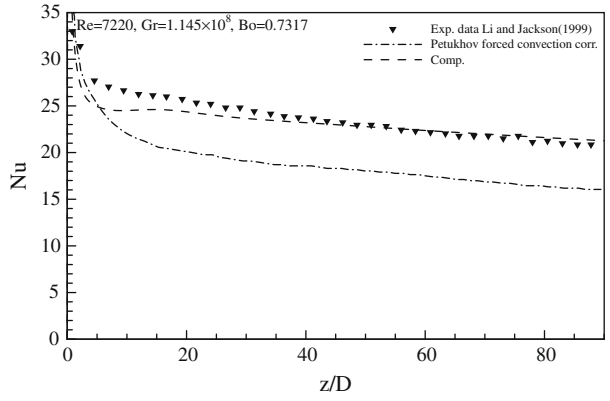


**Fig. 10.** Comparison of predicted Nusselt number from the current model with experimental data for downward flow.

such as inertia and viscosity. Thus, the effect of buoyancy force for this case should not be significant. However, the difference between upward and downward flows should be appreciated.

The computed velocity profiles normalized with the bulk fluid velocity ($U_b$) at various stations along the tube are presented in Fig. 6. At the inlet of the tube, due to negligible effect of the buoyancy force, the corresponding profiles are almost identical for both directions. Further downstream as the near-wall fluid warms up, the buoyancy force accelerates the near-wall fluid in upward flow. In contrast, for downward flow, the buoyancy force acts in the opposite direction of the main stream and slows down the near-wall fluid. As flow approaches the end of the tube ($z/D = 60$), differences in the velocity profiles become more visible and finally both flows reach to the fully-developed condition.

Although one would expect higher heat transfer rates for upward flow compared to the downward flow due to higher near-wall velocity, the non-dimensionalized temperature profiles, shown in Fig. 7, exhibit exactly opposite behavior. Similar to the velocity profiles, the temperature profiles are identical at the entrance region. Further downstream, the difference between the profiles increases. The normalized temperature profiles for the downward flow change marginally while for the upward flow at

similar sections, they vary significantly. The variations in temperature profiles explain the distribution of Nusselt numbers.

To explain the differences in the levels of heat transfer for the upward and downward flows, the near-wall turbulent kinetic energy profiles are presented in Fig. 8. The square-root of turbulent kinetic energy is normalized using the inlet velocity in this figure. Similar to what has been found for the velocity and temperature profiles, the profiles of turbulent kinetic energy are almost identical for both directions in the entry region. However, as the upward flow develops, the turbulent kinetic energy decreases significantly and indications of laminarization are observed at the last stations ($z/D = 30$ and 60). As a result, the turbulent diffusion is impaired for the corresponding stations and consequently the Nusselt number decreases drastically (Fig. 9).

In contrast for downward flow, the buoyancy force opposes the main stream flow in the regions close to the wall. Eventually, the turbulent kinetic energy increases as the buoyancy effect established (Fig. 8). Thus, the rate of heat transfer is enhanced compared to the forced convection rate as can be seen in Fig. 10. While there are some discrepancies between the predicted local Nusselt numbers of the zonal $k$–$\varepsilon$ model and the experimental data, the predictions are in acceptable agreement with the data of Li and Jackson (1999).

### 5.3. Case (c): strong buoyancy force

The buoyancy force in this case is such strong that in the near-wall region for both upward and downward flows, it becomes the dominant force. The flow parameters are Re = 2133, Gr = $8.247 \times 10^7$ making the buoyancy parameter Bo = 34.3111 which is much higher than the cases (a) and (b). For the upward flow, the buoyancy force acts in the flow direction. Thus, the velocity of the near-wall fluid increases slightly as the fluid warms up. The velocity profile obtains its maximum inflated shape at $z/D \approx 15$, the same section where indication of flow reversal is seen at the core region (Fig. 11). Afterwards, the profile is getting smoother due to the development of thermal boundary layer as well as the propagation of buoyancy effect in the radial direction. However, the velocity maintains its M-shape profile through the end of the tube unlike the downward flow (see Fig. 13, $z/D = 30, 60$).

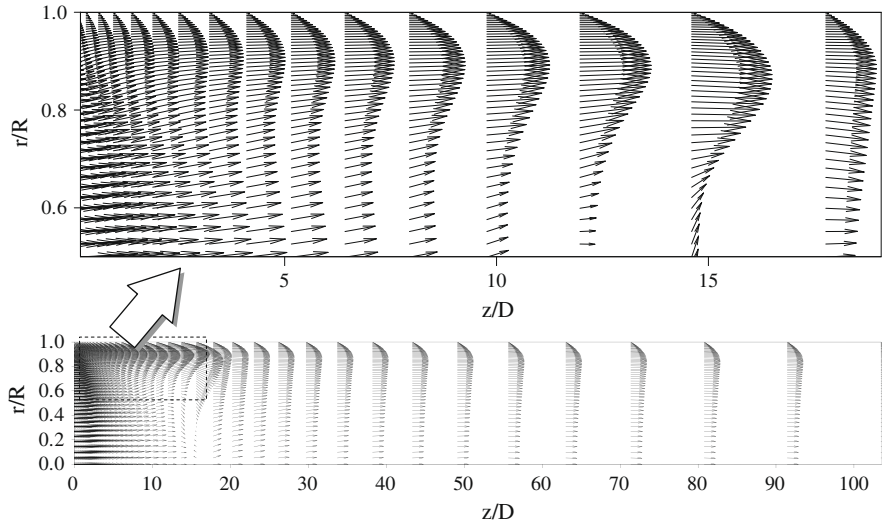


**Fig. 11.** Predicted velocity vectors for upward flow (Re = 2133, Gr = $8.247 \times 10^8$, Bo = 34.3111).

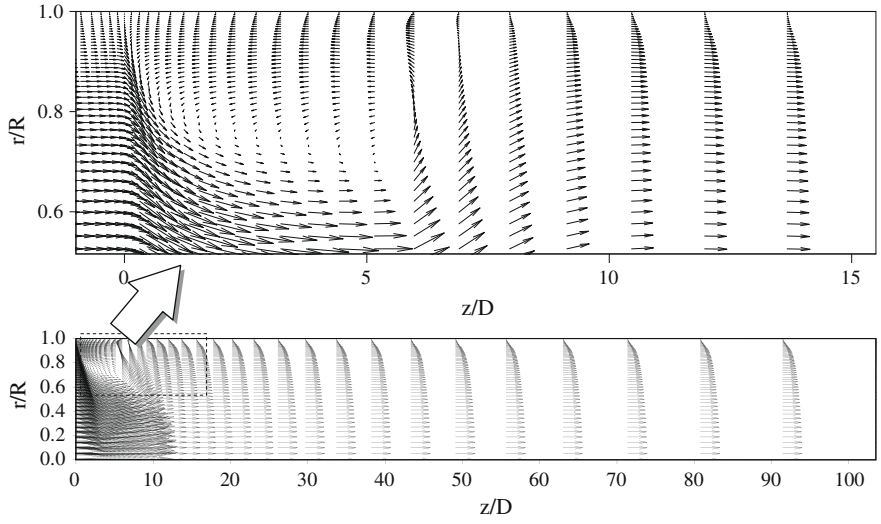


**Fig. 12.** Predicted velocity vectors for downward flow (Re = 2133, Gr = $8.247 \times 10^8$, Bo = 34.3111).

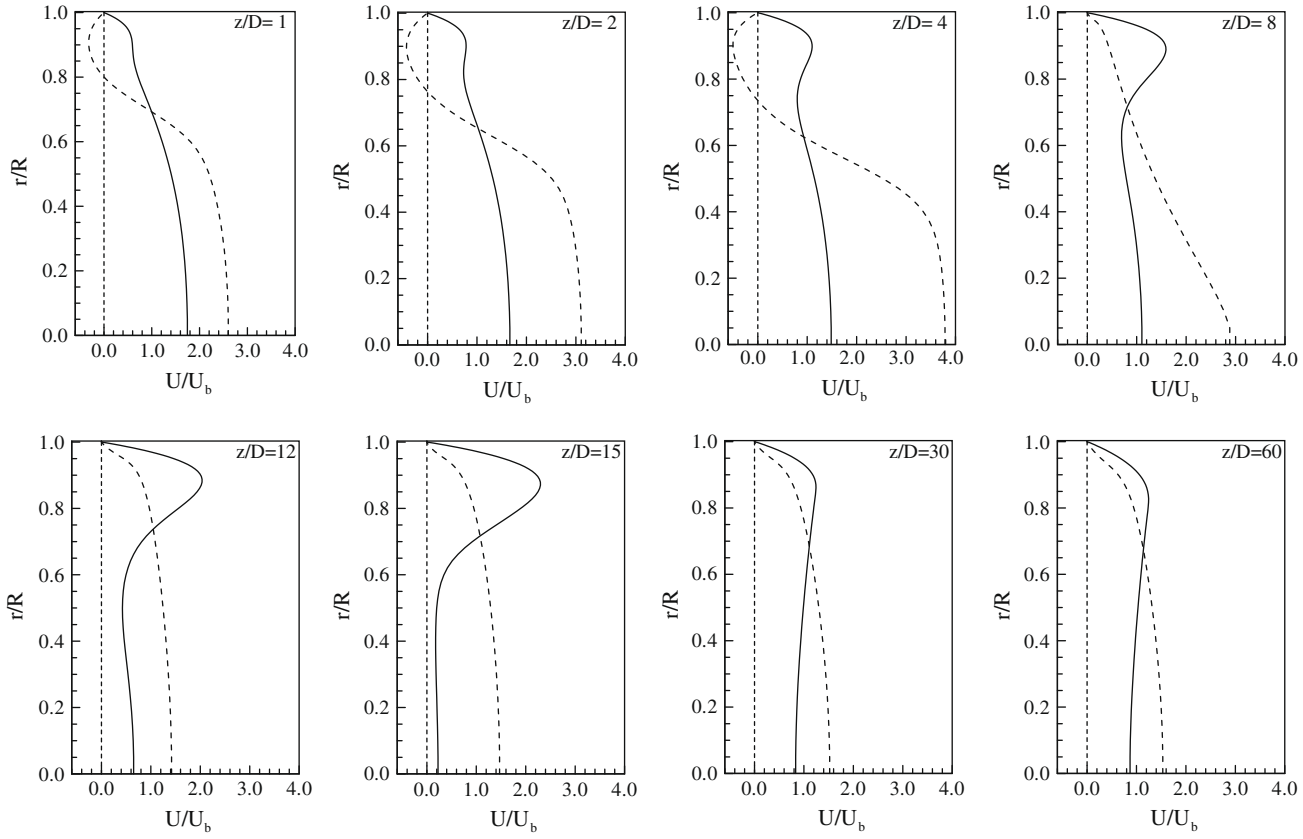


**Fig. 13.** Normalized velocity profiles for upward (solid line) and downward (dashed line) flows at different cross sections (Re = 2133, Gr = $8.247 \times 10^8$, Bo = 34.3111).

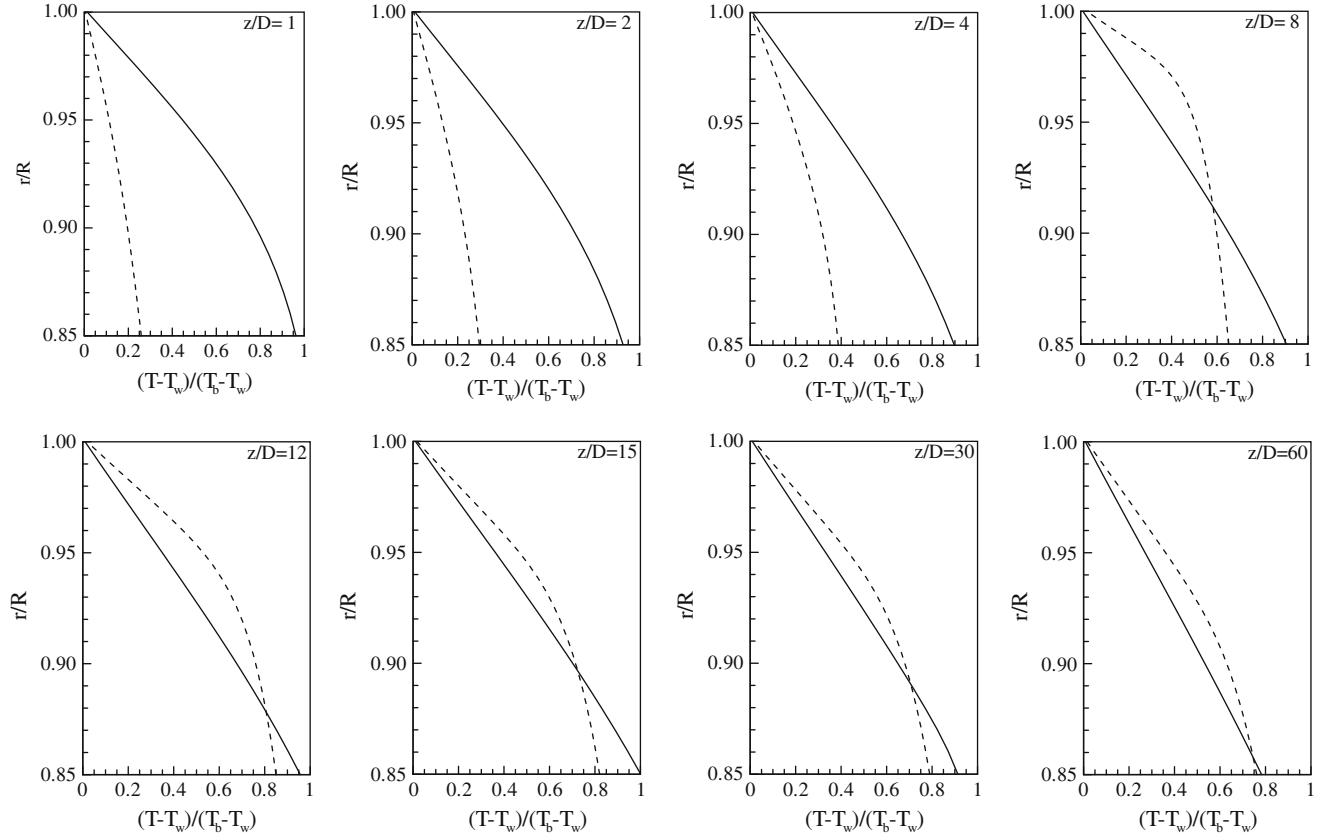


**Fig. 14.** Normalized temperature profiles for upward (solid line) and downward (dashed line) flows at different cross sections (Re = 2133, Gr = $8.247 \times 10^8$, Bo = 34.3111).

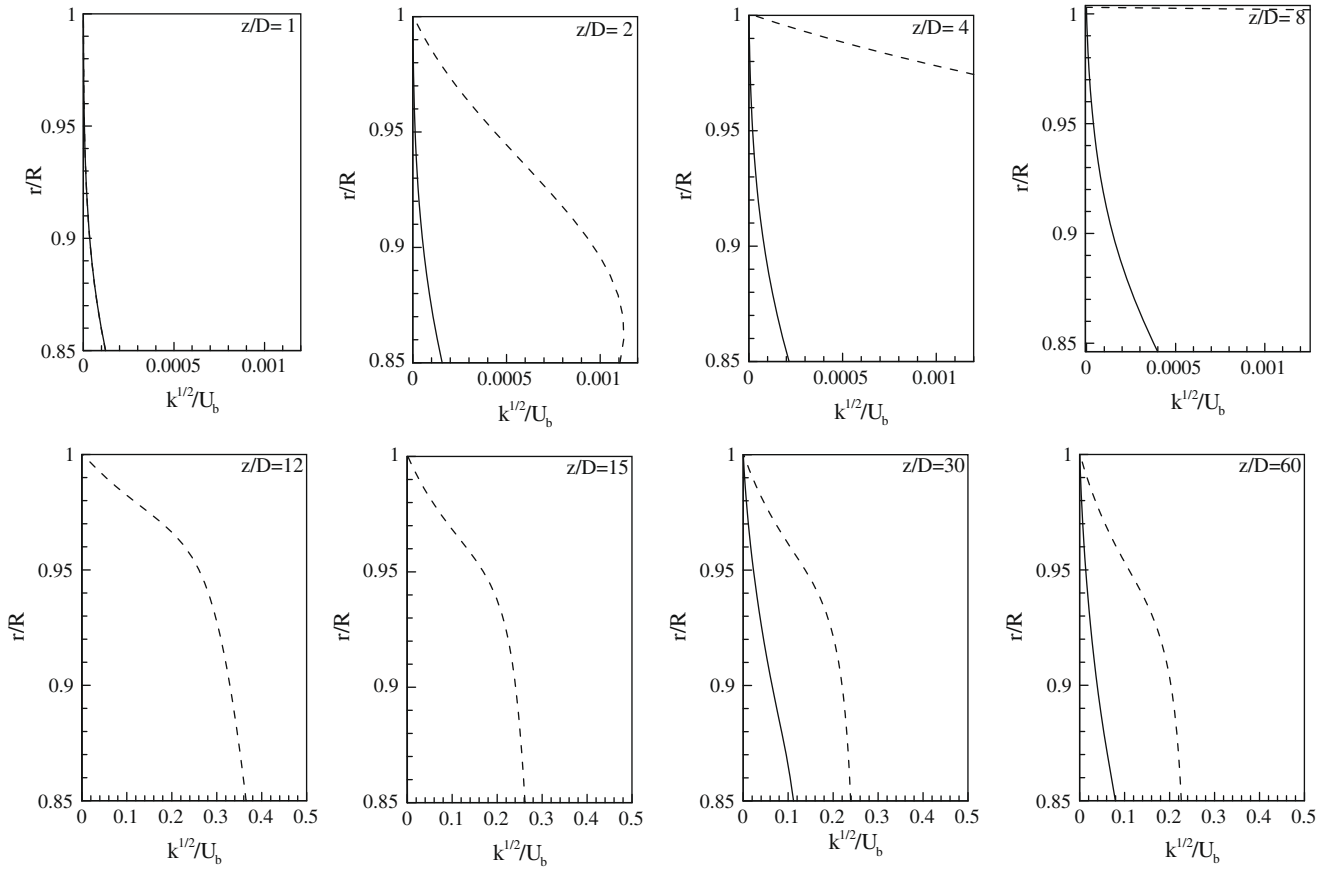


**Fig. 15.** Normalized turbulent kinetic energy profiles for upward (solid line) and downward (dashed line) flows at different cross sections (Re = 2133, Gr = $8.247 \times 10^8$, Bo = 34.3111).

For the downward flow, on the other hand, as the near-wall fluid warms up, it is decelerated by the buoyancy force and the flow reversal occurs. The velocity vectors and the corresponding flow reversal are presented in Fig. 12. The reversed flow develops at the first few stations of the heating zone according to the velocity profiles shown in Fig. 13 ($z/D$ = 1, 2 and 4). Further downstream, due to the increase in the average fluid temperature, flow is rapidly recovered. Consequently, the velocity profiles at the last four sections ($z/D$ = 12, 15, 30 and 60) do not exhibit any significant changes and the flow obtains fully-developed condition.

The corresponding temperature profiles for upward and downward flows are compared in Fig. 14. For the upward flow, as thermal boundary layer grows, heat transfer between the wall and the adjacent fluid is impaired. Further downstream, as the effect of buoyancy appears, the fluid accelerates in the near-wall region as discussed earlier. The inflation in the velocity profile strengthens the convection mechanism leading to enhancement of heat transfer which is observed in the distribution of Nusselt number at $z/D \approx 15$ (Fig. 16). The rate of heat transfer slightly decreases as the flow develops. As opposed to the previous test cases (Bo = 0.0064 and Bo = 0.7317), the levels of Nusselt number are higher than that of pure forced convection confirming that heat transfer can be either impaired by buoyancy or enhanced. This is the established picture of buoyancy-influenced heat transfer in vertical tubes for the buoyancy-aided case.

Fig. 17 shows the distribution of Nusselt number for downward flow. At the onset of heating zone, non-uniformity in the distribution is evident. This unusual behavior is due to the effects of thermal boundary layer and strong buoyancy force acting in combination. The motion of fluid in the near-wall region is retarded by the buoyancy force at the beginning of the heating zone where such influences are significant. This decreases the convection but also leads to an increase in the production of turbulence. As Fig. 15 shows, the turbulent kinetic energy grows rapidly at the first few stations ($z/D$ = 2, 4 and 8). The net effect is that the thermal boundary layer develops more rapidly. Thus, the Nusselt number falls drastically at first and as the thermal layer grows in thickness, the production of additional turbulence due to the buoyancy force becomes considerable. Consequently, the Nusselt number increases and then stabilizes once the thermal development is completed. The value of the local Nusselt number achieves

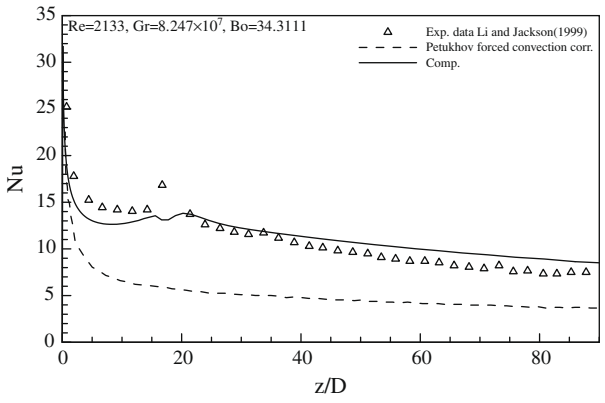


**Fig. 16.** Comparison of predicted Nusselt number from the current model with experimental data for upward flow.

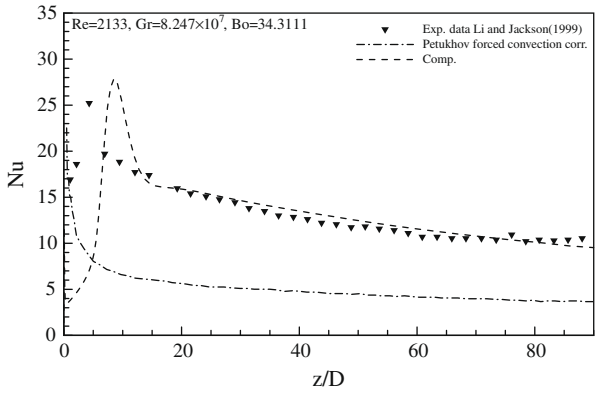


**Fig. 17.** Comparison of predicted Nusselt number from the current model with experimental data for downward flow.

its maximum at the same location where the value of the turbulent kinetic energy is maximized (compare the sections of $z/D \approx 12$ in Figs. 15 and 17).

While the zonal model adopted in this study predicts the correct trends for rate of heat transfer along the tube, it is not able to completely reproduce the variation of local Nusselt number. This suggests that the model overestimates the size of recirculation bubble. However, the numerical results are in satisfactory agreement with experimental data for the fully-developed condition.

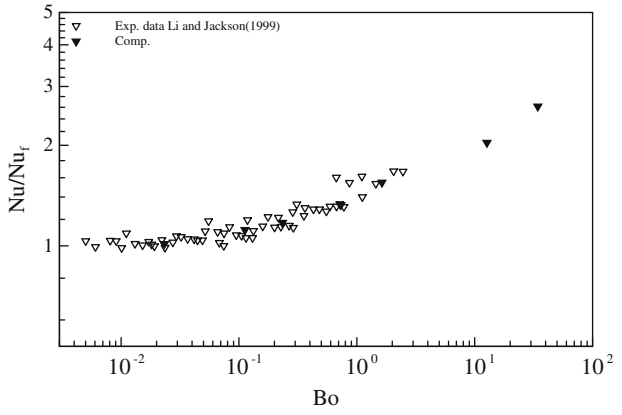


**Fig. 18.** Comparison of the predicted fully-developed Nusselt numbers (at $z/D = 90.3$) with experimental data for downward flow.

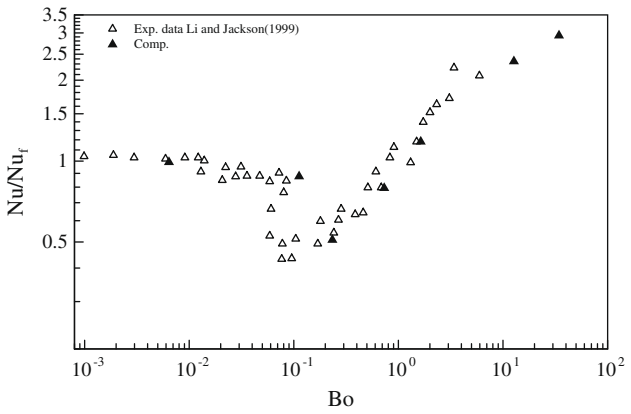


**Fig. 19.** Comparison of the predicted fully-developed Nusselt numbers (at $z/D = 90.3$) with experimental data for upward flow.

### *5.4. Effect of buoyancy on the distribution of fully-developed Nusselt number*

Fig. 18 compares the numerical results for the fully-developed downward flow at $z/D = 90.3$ with the experimental results of Li and Jackson (1999). The Nusselt numbers are normalized using the value of $Nu_f$ for forced convection under the same flow condition. For the downward flow, the buoyancy force always enhances the rate of heat transfer compared to the forced convection. In contrast, for the upward flow, the trend is more readable. As shown in Fig. 19 for this flow, the $Nu/Nu_f$ ratio decreases marginally as the value of buoyancy parameter increases to $Bo \approx 0.09$. A sudden drop of the Nusselt ratio is evident at this particular value of buoyancy parameter ($Bo \approx 0.09$). The rate of heat transfer is recovered as the buoyancy parameter further increases. For condition of strong buoyancy force, where complete laminarization is avoided, local heat transfer is enhanced.

## 6. Conclusions

In this study, numerical computations are performed for turbulent mixed convection in vertical tubes. The flow is studied in both upward and downward directions using the zonal $k$–$\varepsilon$ model. In general, the numerical results are in good agreement with the experiment of Li and Jackson (1999). For downward flow, the buoyancy force acts in opposite direction of the main fluid flow and regardless of the magnitude of the force, buoyancy enhances the rate of heat transfer compared to forced convection in the same condition. Previous studies for laminar flow (Raisee and Shahraeeni, 2007) showed that for downward flow, due to the reduction of the near-wall velocity, the rate of heat transfer is impaired. In the same sense, for turbulent flow, the buoyancy force decelerates the near-wall fluid which weakens convection in this region. For the condition of strong buoyancy force, a flow reversal is also observed. However, the rate of turbulent production is increased in the same region which results in the enhancement of heat transfer.

In contrast to the downward flow, there is no general conclusion for upward flow in terms of enhancement or impairment of heat transfer due to buoyancy. While for downward flow, the buoyancy force always enhances the rate of heat transfer, depending on its magnitude, the buoyancy force may enhance or impair heat transfer. For the negligible buoyancy force, the heat transfer rate is similar to that of forced convection. By increasing the buoyancy parameter up to the value of 0.09, the Nusselt number decreases dramatically. The decrease in the level of Nusselt number is associated with the reduction of turbulence production rate in the near-wall region. Further increase of the Bo parameter results in the enhancement of heat transfer. Eventually, the rate of heat transfer for the upward and downward flows asymptotically gets close to each other for the condition of strong buoyancy force.

The results show that for all buoyancy parameter the zonal $k$–$\varepsilon$ model is accurate for the prediction of turbulent mixed convection in vertical tubes. However, for higher values of the buoyancy parameters, the zonal model only reproduces the Nusselt number for the fully-developed region accurately. For high values of buoyancy parameter, the model successfully predicts the occurrence of a maximum in the Nusselt number distribution, though there are some discrepancies for the location of this point compared to the experimental data.

## References

Bae, J.H., Yoo, J.Y., Choi, H., 2005. Direct numerical simulations of turbulent supercritical flows with heat transfer. Phys. Fluids 17, 105104.

Behzadmehr, A., Galanis, N., Laneville, A., 2003. Low-Reynolds-number mixed convection in vertical tubes with uniform wall heat flux. Int. J. Heat Mass Trans. 46, 4823–4833.

Carr, A.D., Connor, M.A., Buhr, H.O., 1973. Velocity, temperature and turbulence measurements in air for pipe flow with combined free and forced convection. Trans. ASME C, J. Heat Trans. 95, 445–452.

Chien, K.Y., 1982. Predictions of channel and boundary-layer flows with a low-Reynolds-number turbulence model. AIAA J. 20, 33–38.

Cotton, M.A., 1987. Theoretical Studies of Mixed Convection in Vertical Tubes. Ph.D. Thesis, The University of Manchester.

Cotton, M.A., Jackson, J.D., 1990. Vertical tube air flows in the turbulent mixed convection regime calculated using a low-Reynolds-number $k$–$\varepsilon$ model. Int. J. Heat Mass Trans. 33, 275–286.

Cotton, M.A., Kirwin, P.J., 1995. A variant of the low-Reynolds-number two-equation turbulence model applied to variable property mixed convection flows. Int. J. Heat Fluid Flow 16, 486–492.

Iacovides, H., Chew, J.W., 1993. The computation of convective heat transfer in rotating cavities. Int. J. Heat Fluid Flow 14, 146–154.

Iacovides, H., Theofanopoulos, I.P., 1991. Turbulence modelling of axisymmetric flow inside rotating cavities. Int. J. Heat Fluid Flow 12, 2–11.

Jackson, J.D., Cotton, M.A., Axcell, B.P., 1989. Studies of mixed convection in vertical tubes. Int. J. Heat Fluid Flow 10, 2–14.

Kasagi, N., Nishimura, M., 1997. Direct numerical simulation of combined forced and natural turbulent convection in a vertical plane channel. Int. J. Heat Fluid Flow 18, 88–99.

Kenjeres, S., Gunarjo, S.B., Hanjalic, K., 2005. Contribution to elliptic relaxation modelling of turbulent natural and mixed convection. Int. J. Heat Fluid Flow 26, 569–586.

Kim, W.S., He, S., Jackson, J.D., 2008. Assessment by comparison with DNS data of turbulence models used in simulations of mixed convection. Int. J. Heat Mass Trans. 51, 1293–1312.

Launder, B.E., Sharma, B.L., 1974. Application of the energy-dissipation of turbulence to calculation of low near a spinning disc. Lett. Heat Mass Trans. 1, 131–138.

Li, J., Jackson, J.D., 1999. Buoyancy-influenced variable property turbulent heat transfer to air flowing in a uniformly heated vertical tube. In: 2nd EF Conference on Turbulent Heat Transfer, Manchester.

Mikielewicz, D.P., 1994. Comparative Studies of Turbulence Models Under Conditions of Mixed Convection with Variable Properties in Heated Vertical Tubes. Ph.D. Thesis, The University of Manchester.

Petukhov, B.S., Kurganov, V.A., Gladuntsov, A.I., 1972. Turbulent heat in tubes to gases with variable physical properties. Int. J. Heat Mass Trans. 1, 117–127.

Raisee, M. 1999. Computation of Flow and Heat Transfer Through Two- and Three-dimensional Rib-roughened Passages. Ph.D. Thesis, Department of Mechanical Engineering, UMIST.

Raisee, M., Shahraeeni, M., 2007. Numerical simulation of laminar mixed convection of air flow through uniformly heated vertical tubes. In: ASME-JSME Therm. Eng. Summer Heat Transfer Conf., Vancouver, BC, Canada.

Raisee, M., Alemi, H., Iacovides, H., 2006. Prediction of developing turbulent flow in curved ducts using linear and non-linear models. Int. J. Numer. Meth. Flow 56, 1379–1405.

Reichardt, H., 1961. The principles of turbulent heat transfer. Recent Advances in Heat and Mass Transfer. Mc-Graw-Hill, New York. pp. 223–252.

Rhie, C.M., Chow, W.L., 1983. Numerical study of the turbulent flow past an airfoil with trailing edge separation. AIAA J. 21, 1525–1532.

Steiner, A.A., 1971. On the reverse transition of turbulent flow under the action of buoyancy forces. J. Fluid Mech. 47, 71–75.

Sutherland, W., 1893. The viscosity of gases and molecular force. Philos. Mag. 36, 507–531.

Tanaka, H., Maruyama, S., Hatano, S., 1987. Combined forced and natural convection heat transfer for upward flow in a uniformly heated vertical pipe. Int. J. Heat Mass Trans. 30, 165–174.

Wolfshtein, M., 1969. The velocity and temperature distribution in one-dimensional flow with turbulence augmentation and pressure gradient. Int. J. Heat Mass Trans. 12, 301–318.

You, J., Yoo, J.Y., Choi, H., 2003. Direct numerical simulation of heated vertical air flows in fully developed turbulent mixed convection. Int. J. Heat Mass Trans. 46, 1613–1627.